Advances in Engineering Software 100 (2016) 32–42

Contents lists available at ScienceDirect

Advances in Engineering Software

journal homepage: www.elsevier.com/locate/advengsoft

A new boundary meshfree method for potential problems

Fang-Ling Sun[a], Yao-Ming Zhang[a,*], Der-Liang Young[b], Wen Chen[c]

[a] Institute of Applied Mathematics, Shandong University of Technology, Zibo 255049, Shandong, China
[b] Department of Civil Engineering and Hydrotech Research Institute, National Taiwan University, Taipei 10617, Taiwan
[c] Department of Engineering Mechanics, Hohai University, Nanjing 210098, China

ARTICLE INFO

Article history:
Received 31 March 2016
Revised 18 June 2016
Accepted 19 June 2016

Keywords:
Average source method (ASM)
'Completely' regularized boundary integral equation (CRBIE)
Average source technique (AST)
Potential problem

ABSTRACT

This work presents a new boundary meshfree method, named the average source method (ASM), for solving two-dimensional potential problems. The method is based on combining a 'completely' regularized boundary integral equation (CRBIE) with indirect unknowns developed in this paper, removing the singularity computation, and an average source technique (AST). In this approach there are two critical developments. One is the presentation of a new removal singularity technique that results in the CRBIE, and therefore all diagonal coefficients of influence matrices can be evaluated analytically by the off-diagonal ones, unlike some existing meshless boundary approaches that determine diagonal coefficients from the fundamental solution by using a known solution, thereby doubling the solution procedure. The other is to introduce an AST, by which the distributed source on a segment/cell can be reduced to the concentrated point source and therefore the boundary integrals in the CRBIE are not necessary. Hence, in the ASM only boundary nodes are required for computation without involving any integration and element notion. Several benchmark test examples are presented to demonstrate the accuracy, convergence, efficiency and robustness of this new meshfree boundary-node methodology.

1. Introduction

As is known to all, the finite element method (FEM) and boundary element method (BEM) have been the dominant numerical engines for science and engineering applications [1–8,36]. However, they require resorting to an element frame for interpolants of primary variables and the 'energy' integration and thus, depend on the generation of meshes, which can be arduous, time-consuming and even subjected to pitfalls, especially for complex geometry domains. These difficulties can be sidestepped via the so-called meshless/meshfree techniques, which have drawn growing attention during the past decades and achieved outstanding progress in solving a wide class of boundary value problems [8–35].

Among the aforementioned studies, the meshless boundary methods have achieved remarkable progress and can be roughly sorted into two categories: the MFS-based type and the BIE-based type. The former is based on the concept of the method of fundamental solution (MFS), including, but are not limited to, the MFS [12–14], the boundary knot method (BKM) [15–16], the boundary collocation method (BCM) [17], the modified MFS (MMFS) [18], the boundary distributed source method (BDSM) [19–20], the regularized meshless method (RMM) [21–22], and the singular boundary method (SBM) [23–25]. The MFS, BKM and BCM generally lead to the ill-conditioned system. The MMFS and the BDSM need to compute some particular integrals to determine the diagonal terms. The RMM uses double layer kernel to express the potential to easily remove the singularity, but the bewildering hyper singularity issue has to be faced when the boundary flux solutions are required. The SBM uses the null-field integral identity firstly to obtain the diagonal terms from the derivative of the fundamental solution, and then it applies a known solution to determine the diagonal terms from the fundamental solution [23–25]. Therefore, as stated in Ref. [19], this approach amounts to solving the problem twice. In addition, the theoretical analysis of this approach is not rigorous, since it uses a false integral identity [23–25]: $\int_\Gamma \frac{\partial u^{*c}(\boldsymbol{x},\boldsymbol{y})}{\partial \boldsymbol{n}(\boldsymbol{y})} d\Gamma(\boldsymbol{y}) = 0, \boldsymbol{x} \in \Gamma$ with $u*^c(\boldsymbol{x}, \boldsymbol{y})$ beings the fundamental solution of the exterior problems. The latter category [8–11,26–31] is based on combining BIEs with meshless shape functions constructed usually by using the moving least-square (MLS) approximation. It is mainly represented by the boundary node method (BNM) [26] and its variants [27–31]. These methods exploit the merits of both the BIE in dimensionality reduction and the MLS in element removal. The essential difference between these methods consists in the construction of meshless shape functions. Anyhow, they still require the calculation of boundary integrals.

Inspired by the pioneering work, this study presents a new meshfree boundary method for 2D potential problems. The method

* Corresponding author.
E-mail address: zymwfc68@163.com (Y.-M. Zhang).

http://dx.doi.org/10.1016/j.advengsoft.2016.06.009
0965-9978/

is based on combing a CRBIE with direct unknowns developed in this paper, which excludes the computation of both the weakly and strongly singular integrals, with the AST. By using the CRBIE to avoid the singularity of the kernel functions, the major challenge of the coincidence of the source and collocation points vanishes. By introducing the AST into the CRBIE, the distributed source on a segment/cell can be reduced to the concentrated point source and therefore the boundary integrals are no longer required. Since no known solution in the MMFS, RMM and SBM is applied for computing indirectly the diagonal coefficients of influence matrices, the problem can be solved only once with the present approach. Again, unlike the foregoing MLS-based methods [26–31] which is based on introducing MLS-based meshless shape functions constructed elaborately into BIEs and is 'truly meshless' but still involves the calculation of boundary integrals, the present ASM only requires boundary nodes for computation without involving any element or integration notion. Consequently, the ASM is easier-to-implement, much more computationally efficient, and theoretically simpler. Furthermore, in the implementation of the ASM, the real geometry of the domain boundary without approximation can be employed for computation as long as the parametric representation of the domain boundary is given.

As usual, the ASM also requires the discretization of the domain boundary into cells, but as stated in Ref. [28], the using of the cells should not be viewed as a shortcoming of meshless/meshfree schemes if these cells can be generated with ease. Actually, the cells in the ASM are essentially distinguished from the boundary elements in BEM and are employed neither for the purpose of interpolation of the primary variables nor for numerical integration just for computing the Jacobian value at nodes, and also there is no limitation on their shape and size, implying that when some of them are partitioned into smaller cells, their adjacent ones are not affected. In this sense, the ASM should be regarded as a "truly meshless or meshfree" method.

The accuracy, stability, efficiency and widely practical applicability are verified in numerical experiments of the Dirichlet and mixed-type continue or discontinue boundary conditions (BCs) of both interior and exterior problems with simple and complicated boundaries.

2. Regularized BIEs and the ASM

In this paper, we always assume that Ω is a bounded domain in R^2, Ω^c its open complement, and Γ their common boundary.

2.1. Boundary value problem

Consider a two-dimensional potential problem in the domain $\hat{\Omega}$ ($\hat{\Omega}=\Omega$ or Ω^c) governed by the Laplace equation

$$\nabla^2 u(\boldsymbol{x})=0,\quad \boldsymbol{x}=(x_1,x_2)\in\hat{\Omega} \tag{1}$$

with boundary conditions (BCs) [1–2,5–7]

$$u(\boldsymbol{x})=\bar{u}(\boldsymbol{x}),\quad \boldsymbol{x}\in\Gamma_1 \tag{2}$$

$$q(\boldsymbol{x})=\frac{\partial u(\boldsymbol{x})}{\partial \boldsymbol{n}(\boldsymbol{x})}=\bar{q}(\boldsymbol{x}),\quad \boldsymbol{x}\in\Gamma_2 \tag{3}$$

when $\hat{\Omega}=\Omega^c$, in order to guarantee the uniqueness of solution of the exterior problems, the following infinity condition must be supplemented [7,33]

$$|u(\boldsymbol{x})|=O(1),\ \text{as}\ \rho=\sqrt{x_1^2+x_2^2}\to\infty \tag{4}$$

where $\Gamma=\Gamma_1\cup\Gamma_2$ is the boundary of $\hat{\Omega}$ with $\Gamma_1\cap\Gamma_2=\emptyset$; $\bar{u}(\boldsymbol{x})$ and $\bar{q}(\boldsymbol{x})$ are the prescribed boundary functions and $\boldsymbol{n}(\boldsymbol{x})$ is the unit outward normal vector at point $\boldsymbol{x}=(x_1,x_2)\in\Gamma$.

2.2. Regularized indirect boundary integral equations *(IBIEs)*

For potential problems in the domain $\hat{\Omega}$ ($=\Omega$ or Ω^c) bounded by boundary Γ, in the absence of body source, the equivalent regularized IBIEs for the problems (1)–(4) can be expressed as [7,33]

$$\int_\Gamma \phi(\boldsymbol{x})d\Gamma=0 \tag{5}$$

$$u(\boldsymbol{y})=\int_\Gamma \phi(\boldsymbol{x})u^*(\boldsymbol{x},\boldsymbol{y})d\Gamma+C,\quad \boldsymbol{y}\in\Gamma \tag{6}$$

$$\frac{\partial u(\boldsymbol{y})}{\partial \boldsymbol{n}_{\boldsymbol{y}}}=\hat{k}\phi(\boldsymbol{y})+\int_\Gamma[\phi(\boldsymbol{x})-\phi(\boldsymbol{y})]\frac{\partial u^*(\boldsymbol{x},\boldsymbol{y})}{\partial \boldsymbol{n}_{\boldsymbol{y}}}d\Gamma+\phi(\boldsymbol{y})\int_\Gamma\left[\frac{\partial u^*(\boldsymbol{x},\boldsymbol{y})}{\partial \boldsymbol{n}_{\boldsymbol{y}}}+\frac{\partial u^*(\boldsymbol{x},\boldsymbol{y})}{\partial \boldsymbol{n}_{\boldsymbol{x}}}\right]d\Gamma,\quad \boldsymbol{y}\in\Gamma \tag{7}$$

$$\frac{\partial u(\boldsymbol{y})}{\partial \boldsymbol{t}_{\boldsymbol{y}}}=\int_\Gamma[\phi(\boldsymbol{x})-\phi(\boldsymbol{y})]\frac{\partial u^*(\boldsymbol{x},\boldsymbol{y})}{\partial \boldsymbol{t}_{\boldsymbol{y}}}d\Gamma+\phi(\boldsymbol{y})\int_\Gamma\left[\frac{\partial u^*(\boldsymbol{x},\boldsymbol{y})}{\partial \boldsymbol{t}_{\boldsymbol{y}}}+\frac{\partial u^*(\boldsymbol{x},\boldsymbol{y})}{\partial \boldsymbol{t}_{\boldsymbol{x}}}\right]d\Gamma,\quad \boldsymbol{y}\in\Gamma \tag{8}$$

For the internal point $\boldsymbol{y}\in\hat{\Omega}$, the integral equations can be written as

$$u(\boldsymbol{y})=\int_\Gamma \phi(\boldsymbol{x})u^*(\boldsymbol{x},\boldsymbol{y})d\Gamma+C,\quad \boldsymbol{y}\in\hat{\Omega} \tag{9}$$

$$\frac{\partial u(\boldsymbol{y})}{\partial y_k}=\int_\Gamma \phi(\boldsymbol{x})\frac{\partial u^*(\boldsymbol{x},\boldsymbol{y})}{\partial y_k}d\Gamma,\quad \boldsymbol{y}\in\hat{\Omega},k=1,2 \tag{10}$$

In Eqs. (5)–(10), $\boldsymbol{x}=(x_1,x_2)$ and $\boldsymbol{y}=(y_1,y_2)$ are the source and the field points, respectively; $\boldsymbol{t}_{\boldsymbol{y}}=(t_1(\boldsymbol{y}),t_2(\boldsymbol{y}))$ and $\boldsymbol{n}_{\boldsymbol{y}}=(n_1(\boldsymbol{y}),n_2(\boldsymbol{y}))$ are the unit tangent and outward normal vectors at $\boldsymbol{y}\in\Gamma=\partial\hat{\Omega}$; $\hat{k}$ is 1 or 0, respectively, for the interior domain Ω and the exterior domain Ω^c; $u*(\boldsymbol{x},\boldsymbol{y})$ denotes the fundamental solution for potential problems expressed as

$$u^*(\boldsymbol{x},\boldsymbol{y})=-\frac{1}{2\pi}\ln|\boldsymbol{x}-\boldsymbol{y}| \tag{11}$$

In order to sidestep the direct computation of the weak singular integral in Eq.(6), based on the following integral identities

$$\int_\Gamma n_i(\boldsymbol{x})u^*(\boldsymbol{x},\boldsymbol{y})d\Gamma=\int_\Gamma (x_i-y_i)\frac{\partial u^*(\boldsymbol{x},\boldsymbol{y})}{\partial \boldsymbol{n}}d\Gamma,\boldsymbol{y}\in\hat{\Omega},i=1,\cdots,d \tag{12}$$

which is readily derived by the Green' second identity, and a limit procedure, i.e.

Lemma [33–35]. *Let Γ be a piecewise smooth curve (open or closed), and $\hat{\boldsymbol{x}}$ a point on Γ (perhaps a corner). Suppose $h=|\boldsymbol{y}-\hat{\boldsymbol{x}}|$ and $d=\inf_{\boldsymbol{x}\in\Gamma}|\boldsymbol{y}-\boldsymbol{x}|$. If $\psi(\boldsymbol{x})\in C^{0,\alpha}(\Gamma)$ and $h/d\le K_1$(with constant K_1), then there holds*

$$\lim_{\boldsymbol{y}\to\hat{\boldsymbol{x}}}\int_\Gamma\frac{x_k-y_k}{|\boldsymbol{x}-\boldsymbol{y}|^2}[\psi(\boldsymbol{x})-\psi(\hat{\boldsymbol{x}})]d\Gamma_{\boldsymbol{x}}=\int_\Gamma\frac{x_k-\hat{x}_k}{|\boldsymbol{x}-\hat{\boldsymbol{x}}|^2}[\psi(\boldsymbol{x})-\psi(\hat{\boldsymbol{x}})]d\Gamma_{\boldsymbol{x}}\quad(k=1,2)$$

we develop a new boundary element formulation as follows

$$u(\boldsymbol{y})=\int_\Gamma[\phi(\boldsymbol{x})-\phi(\boldsymbol{y})\boldsymbol{n}(\boldsymbol{y})\cdot\boldsymbol{n}(\boldsymbol{x})]u^*(\boldsymbol{x},\boldsymbol{y})d\Gamma+\phi(\boldsymbol{y})\int_\Gamma\boldsymbol{n}(\boldsymbol{y})\cdot(\boldsymbol{x}-\boldsymbol{y})\frac{\partial u^*(\boldsymbol{x},\boldsymbol{y})}{\partial \boldsymbol{n}_{\boldsymbol{x}}}d\Gamma+C,\boldsymbol{y}\in\Gamma \tag{13}$$

which is named the 'completely' regularized boundary integral equation, because it excludes the computation of both the weakly and strongly singular integrals.

2.3. Formulations of the ASM

In this section, an average source technique is proposed, by which the distributed source on a segment/ cell can be reduced to the concentrated point source and therefore the boundary integrals are not necessary. Assume that $f(\boldsymbol{x}, \boldsymbol{y})$ represents the integrand of the integrals in the above Eqs. (5), (7)–(10) and (13). Then, when $\boldsymbol{y} \notin \Gamma_j$, $f(\boldsymbol{x}, \boldsymbol{y})$ is a smooth function with respect to $\boldsymbol{x}$ on the Γ_j, and thus by utilizing the mean value theorem, we have

$$\int_{\Gamma_j} f(\boldsymbol{x}, \boldsymbol{y}) d\Gamma_{\boldsymbol{x}} = f(\boldsymbol{x}_A, \boldsymbol{y}) l_j \tag{14}$$

where $f(\boldsymbol{x}_A, \boldsymbol{y})$ is be referred to as an average source of distributed source on segment Γ_j. In practical application, boundary point $\boldsymbol{x}_A$ can be replaced by boundary nodes $\boldsymbol{x}_j$ on Γ_j (usually the mid-point of the segment Γ_j) since the dimension (e.g., length or area) of each segment is generally very small after boundary discretization. Therefore, Eq. (14) can be rewritten as

$$\int_{\Gamma_j} f(\boldsymbol{x}, \boldsymbol{y}) d\Gamma_{\boldsymbol{x}} = \int_{-1}^{1} f(\boldsymbol{x}(\xi), \boldsymbol{y}) J(\xi) d\xi \approx \omega_j f(\boldsymbol{x}_j, \boldsymbol{y}) \tag{15}$$

where $\boldsymbol{x}_j$ is the mid-point of the segment Γ_j, and $\omega_j = 2J(\boldsymbol{x}_j)$, where $J(\boldsymbol{x}_j)$ is the Jacobian value at the jth node $\boldsymbol{x}_j$.

When $\boldsymbol{y} = \boldsymbol{x}_j \in \Gamma_j$, based on the AST, we have

$$\int_{\Gamma_j} \left[\frac{\partial u^*(\boldsymbol{x}, \boldsymbol{y})}{\partial \boldsymbol{n}_{\boldsymbol{y}}} + \frac{\partial u^*(\boldsymbol{x}, \boldsymbol{y})}{\partial \boldsymbol{n}_{\boldsymbol{x}}} \right] d\Gamma \approx -\kappa(\boldsymbol{x}_j) \omega(\boldsymbol{x}_j)$$

in which $\kappa(\boldsymbol{x}_j)$ is the curvature of the boundary at the node $\boldsymbol{x}_j$, and $\omega(\boldsymbol{x}_j) = \frac{1}{\pi} J(\boldsymbol{x}_j)$, with $J(\boldsymbol{x}_j)$ being the value of the Jacobian at jth node $\boldsymbol{x}_j$.

In a similar way, the other integrals in the above Eqs.(5), (7)–(10) and (13) can also be reduced to the boundary node form. Therefore, Eqs. (5), (7), (8) and (13) can be expressed as

$$\sum_{j=1}^{N} J(\boldsymbol{x}_j) \phi_j = 0 \tag{16}$$

$$u_i = \sum_{j=1}^{N} (G_{ij} \phi_j) \tag{17}$$

$$q_i^n = \sum_{j=1}^{N} (H_{ij}^n \phi_j) \tag{18}$$

$$q_i^t = \sum_{j=1}^{N} (H_{ij}^t \phi_j) \tag{19}$$

where N is the total number of collocation points on all cells, ϕ_j the unknown density at the jth node, and G_{ij}, H_{ij}^n and H_{ij}^t are influence coefficients corresponding to Eq. (13), (7) and (8), respectively, given by

$$G_{ij} = \begin{cases} -\omega_j \ln r_{ij}, i \neq j \\ \sum\limits_{k=1, k \neq i}^{N} \boldsymbol{n}_i \cdot \boldsymbol{n}_k \omega_k \ln r_{ik} \\ \quad - \sum\limits_{k=1, k \neq i}^{N} \boldsymbol{n}_i \cdot (\boldsymbol{x}_k - \boldsymbol{x}_i) \omega_k \dfrac{(\boldsymbol{r}_{ik} \cdot \boldsymbol{n}_k)}{r_{ik}^2}, \quad j = i \end{cases} \tag{20}$$

$$H_{ij}^n = \begin{cases} \omega_j \dfrac{(\boldsymbol{r}_{ij} \cdot \boldsymbol{n}_i)}{r_{ij}^2}, i \neq j \\ \hat{k} - \sum\limits_{k=1, k \neq i}^{N} \omega_k \dfrac{\boldsymbol{r}_{ik} \cdot \boldsymbol{n}_k}{r_{ik}^2} - \omega_i \kappa_i, j = i \end{cases} \tag{21}$$

$$H_{ij}^t = \begin{cases} \omega_j \dfrac{(\boldsymbol{r}_{ij} \cdot \boldsymbol{t}_i)}{r_{ij}^2}, i \neq j \\ - \sum\limits_{k=1, k \neq i}^{N} \omega_k \dfrac{\boldsymbol{r}_{ik} \cdot \boldsymbol{t}_k}{r_{ik}^2}, j = i \end{cases} \tag{22}$$

where $\boldsymbol{r}_{ik}$ is the vector from the ith node to the kth node, r_{ik} is the distance from the ith node to the kth node, $\boldsymbol{t}_k = (t_1^k, t_2^k)$ and $\boldsymbol{n}_k = (n_1^k, n_2^k)$ are the unit tangent and normal vectors to Γ at the kth node, respectively, $\omega_i = \frac{1}{\pi} J(\boldsymbol{x}_i)$, with $J(\boldsymbol{x}_i)$ being the value of the Jacobian at $i$the node $\boldsymbol{x}_i$, and κ_i is the curvature of the boundary at the ith node.

It should be noted that any boundary flux can be calculated by an appropriate combination of the normal gradient Eq. (21) and the tangential gradient Eq. (22).

For any internal point $\boldsymbol{y}$ far from the boundary, by applying the AST, Eqs. (9) and (10) can be reduced to the boundary node form as follows

$$u(\boldsymbol{y}) = -\frac{1}{2\pi} \sum_{j=1}^{N} \phi_j \ln r_{ij} \omega_j + C, \quad \boldsymbol{y} \in \hat{\Omega} \tag{23}$$

$$\frac{\partial u}{\partial y_k}(\boldsymbol{y}) = \sum_{j=1}^{N} \phi_j \frac{r_k}{r_{ij}^2} \omega_k, \quad \boldsymbol{y} \in \hat{\Omega}, k = 1, 2 \tag{24}$$

where $r_k = x_k - y_k$.

3. Numerical examples

In this section, the validity, accuracy and convergence of the proposed method are tested to the potential problems with square, circular, multiply-connected and irregular domains, subjected to various BCs. For all test examples, the true geometry of the boundary without approximation is used for computation.

To assess the accuracy of the proposed ASM, the relative error of the multiple calculation results is defined by

$$\text{Relative error} = \sqrt{\sum_{k=1}^{M} (t_{number}^k - t_{exact}^k)^2 \Big/ \sum_{k=1}^{M} (t_{exact}^k)^2} \tag{25}$$

where M is the total number of calculation points, and t_{number}^k and t_{exact}^k denote the numerical and exact solution at the kth calculation point, respectively..

3.1. Square domain problems with mixed-type bc

Example 1. A square domain($\pi \times \pi$) subject to the mixed-type BC is considered as

$$u(\pi, x_2) = 1, q(x_1, 0) = u(x_1, \pi) = q(0, x_2) = 0 \tag{26}$$

which is an example used in Ref. [21]. An analytical solution is available as follows

$$u(x_1, x_2) = \sum_{n=1}^{\infty} D_n \cosh\left(\frac{(2n-1)x_1}{2}\right) \cos\left(\frac{(2n-1)x_2}{2}\right) \tag{27}$$

where

$$D_n = \frac{4(-1)^{n+1}}{(2n-1)\pi \cosh\left(\frac{(2n-1)\pi}{2}\right)} \tag{28}$$

The field potential solutions by using the analytical results and the proposed ASM are plotted in Fig. 1(a) and (b), respectively with using 120 boundary nodes. It can be seen that results of the ASM match the exact solutions very well. To investigate the error analysis, Fig. 2(a) and (b) show the absolute error surfaces of the

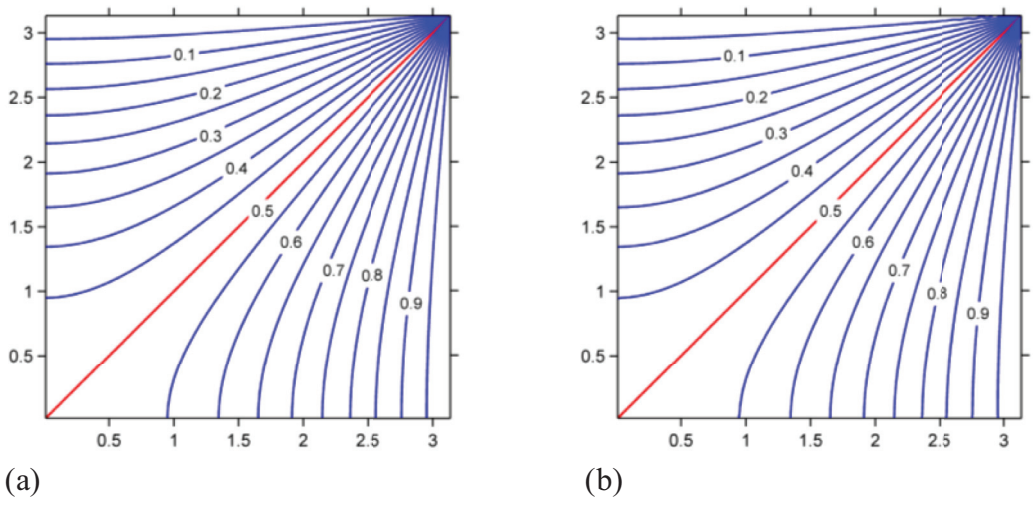

Fig. 1. The field potential solutions: (a) exact results and (b) proposed method (120 source nodes).

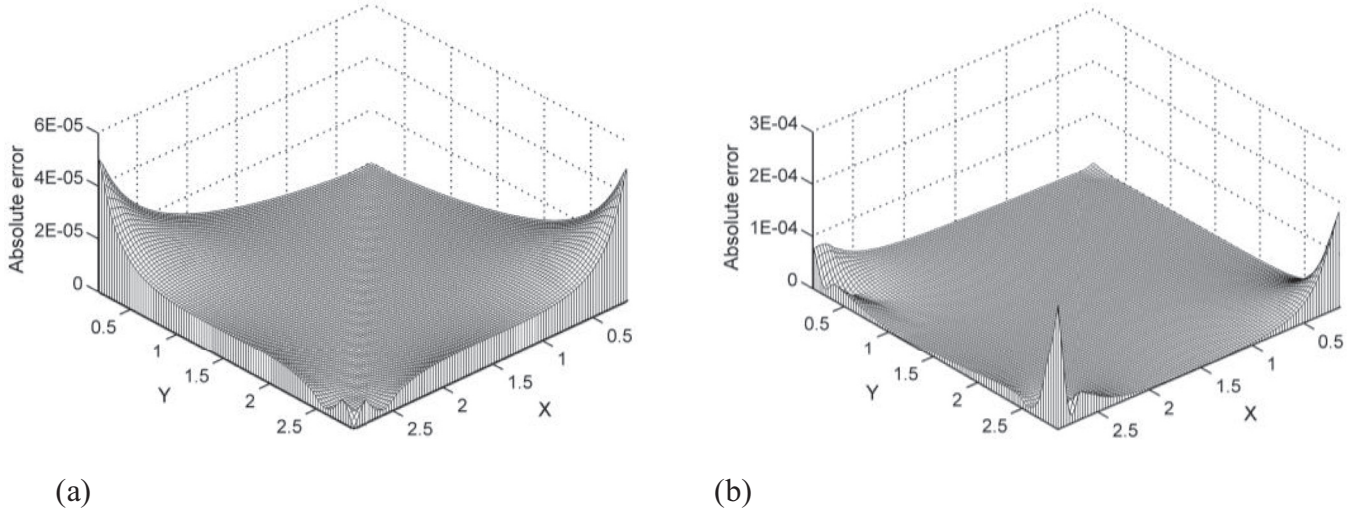

Fig. 2. Absolute error surfaces for field solutions: (a) potential and (b) flux $\partial u/\partial x_1$ (200 nodes).

computational results, respectively, for the potential u and the flux $\partial u/\partial x_1$, in which the absolute errors are generated at 30×30 interior points uniformly distributed over a square domain covering $0.14 \le x_1, x_2 \le 2.9$. These two figures clearly illustrate that the proposed ASM works well for the mixed-type problems.

3.2. Circular domain problems with continue and discontinue BCs

Examples 2 and 3 consider the interior and exterior Dirichlet problems with discontinue BCs, respectively, while Example 4 addresses an interior Dirichlet problem with continue BCs, which is an example used in Ref. [19,24], to make a comparison between the present ASM and other methods.

Example 2. Problem sketch is depicted in Fig. 3, which is an example used in Ref. [21]. The problem is subjected to Dirichlet discontinuous BC as follows:

$$u(1,\varphi) = \begin{cases} 0 & 0 < \varphi < \pi \\ 1 & \pi < \varphi < 2\pi \end{cases} \tag{29}$$

In this case, an analytical solution is available as follows

$$u(x_1,x_2) = \frac{1}{\pi}\arctan\left(\frac{2x_2}{x_1^2+x_2^2-1}\right) + \frac{1}{2} \tag{30}$$

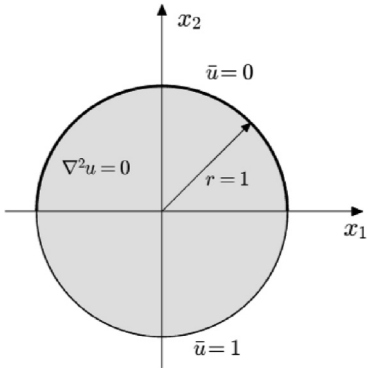

Fig. 3. Problem sketch.

The contour plot of the exact field potential solution is plotted in Fig. 4(a). Fig. 4(b) shows the field solutions calculated by using the proposed method with 60 boundary nodes. Good match is observed from the comparison of Fig. 4(a) and (b). To further investigate the accuracy and the convergence of the proposed ASM, we plot Fig. 5(a)–(c). Fig. 5(a) and (b) display the absolute error surfaces of the potential solutions in the interested

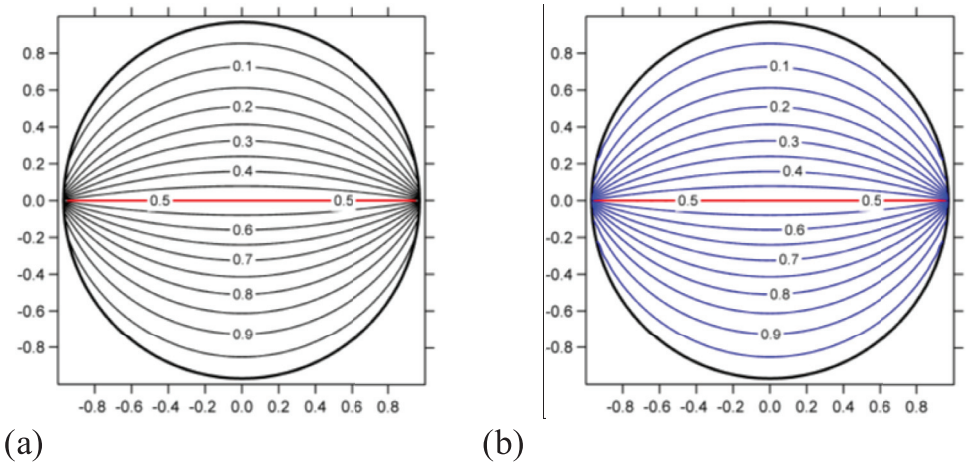

Fig. 4. The contour plots for field potentials: (a) exact and (b) the proposed method (60 nodes).

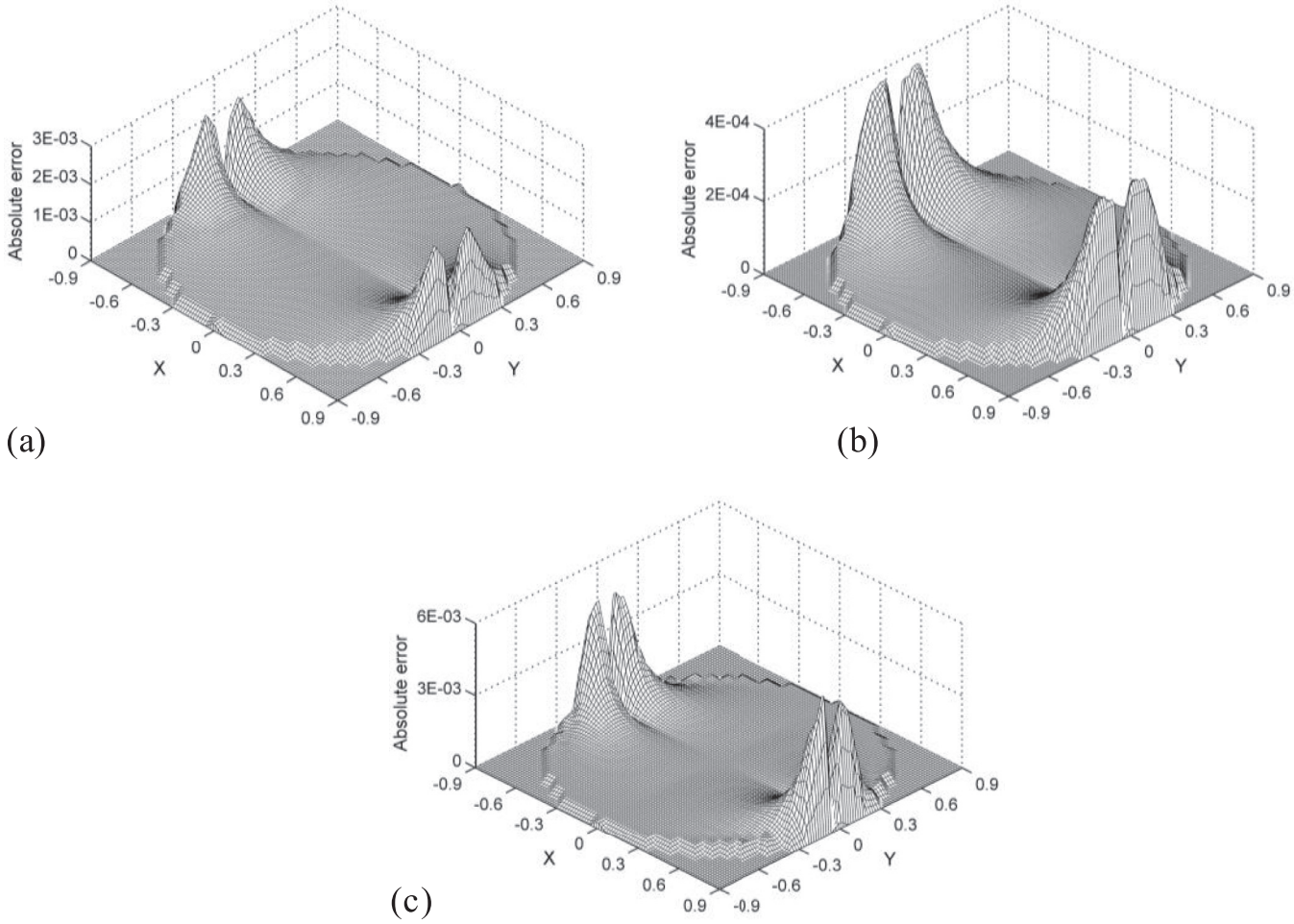

Fig. 5. Absolute error surfaces for field solutions: (a) potential (60 nodes), (b) potential (120 nodes) and (c) flux $\partial u/\partial x_1$ (120 nodes).

domain $\{(\rho, \varphi)$: $0 \le \rho \le 0.9$, $0 \le \varphi \le 2\pi\}$ with 800 interior points using 60 and 120 boundary nodes, respectively. And Fig. 5(c) shows the absolute error surface for the field flux $\partial u/\partial x_1$ in the aforementioned domain with the same number of interior points using 120 source points. Due to discontinuity of BC, it can be seen from these figures that the errors increase when the calculated points are close to the boundary at $\boldsymbol{y} = 0$, and still, acceptable numerical accuracies can be achieved by the present method. Furthermore, we also can see through the comparison of Fig. 5(a) and (b) that the proposed method is stable, accurate, and rapidly convergent as the number of boundary nodes increases. Meanwhile for the purpose of comparison with the Ref. [21], Fig. 6(a) and (b) display the norm error for the potential solution u and the flux solution $q^1 = \partial u/\partial x_1$ along the circle of radius $\rho_0 = 0.5$ and center at the origin versus the number of the boundary nodes by using the ASM, BEM and RMM. The norm errors are defined as $\int_0^{2\pi} |u_{\text{exa}}(\rho_0, \varphi) - u_{\text{num}}(\rho_0, \varphi)|^2 d\varphi$ in Fig. 6(a) and $\int_0^{2\pi} |q^1_{\text{exa}}(\rho_0, \varphi) - q^1_{\text{num}}(\rho_0, \varphi)|^2 d\varphi$ in Fig. 6(b), respectively, which

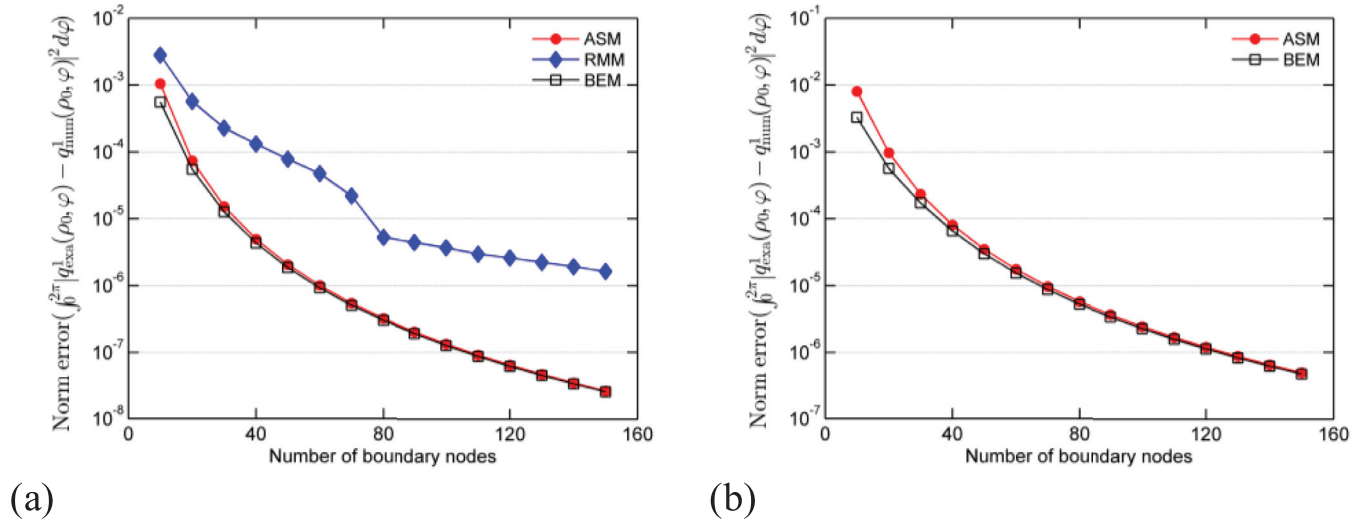

Fig. 6. The norm errors of the solutions along the circle of radius$\rho_0 = 0.5$ vs. the number of nodes: (a) potential and (b) flux $\partial u/\partial x_1$.

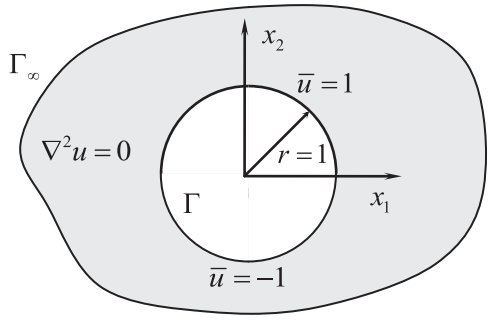

Fig. 7. Problem sketch.

are the same as in Ref. [21]. It can be found that both the ASM and the BEM converge faster than the RMM [21] with the increase of the boundary node number, and meanwhile, the solution accuracy and convergence rates of the former two are very close. It should be noted, however, that the proposed ASM is inherently free from meshing and integration, easier-to-implement, much more computationally efficient, and theoretically simpler. Hence this example further verifies that the ASM works well for discontinuous BC problems.

Example 3. In this case study, we investigate an exterior Dirichlet problem with discontinuous BC [21], whose sketch is depicted in Fig. 7. The BC is imposed on the edge of the unit circular domain and is given as follows:

$$u(1,\varphi) = \begin{cases} 1 & 0 < \varphi < \pi \\ -1 & \pi < \varphi < 2\pi \end{cases} \tag{31}$$

In this case, an analytical solution is available as follows

$$u(x_1, x_2) = \frac{2}{\pi} \arctan\left(\frac{2x_2}{x_1^2 + x_2^2 - 1}\right) \tag{32}$$

60 boundary nodes, uniformly distributed with respect to φ on the unit circumference, are used in following calculations. The contour plot of the field potential exact solution is plotted in Fig. 8(a). And Fig. 8(b) shows the numerical results for the field potential by using the proposed ASM. It can be seen from the comparison of these two figures that the results by the ASM are in excellent agreement with the exact solution. Furthermore, Fig. 9(a) and (b) display the relative errors of the computational results obtained by the ASM and BEM, respectively, for the field potential u and its derivative $\partial u/\partial x_1$, at 32 field points uniformly distributed on a circle with radius $\rho = 2$ and center at the origin. And Fig. 10 depicts the boundary normal flux $\partial u/\partial \boldsymbol{n}$ solutions at 60 boundary nodes by using the ASM, the BEM and the analytical solutions. Hence we can observe from Fig. 9(a) and (b) and Fig. 10 that high calculation accuracy can be achieved by both the ASM and BEM though with a very small number of boundary nodes. On the other hand, although their accuracies are very close, as shown in the previous test example, the ASM is essentially free of mesh and integration.

Example 4. The test example investigates a circular domain of radius $r = 2$, which is an example used in Ref. [19,24]. Dirichlet BC is imposed on the edge of the circle using the following analytical solution:

$$u(r,\theta) = r^6 \cos(6\theta) \tag{33}$$

in the polar coordinates (r, θ).

The number of boundary nodes used varies from 100 to 1400, which is the same as in Ref. [19,24] to make a fair comparison between these tested methods.

A total number of 120 calculation points are selected inside the domain distributed uniformly on a circle with radius $r = 1$ and center at the origin for the solution of the field potentials. Fig. 11 shows the relative error curves for the field potential solutions at these calculation points by using different numerical methods. Here, the BEM, SBM, BDS and RMM solutions come from Ref. [24].

It can be seen from Fig. 11 that overall, the solution accuracy and convergence rate of the present ASM and the SBM are very close, but with the number of boundary nodes being less than 300, the ASM converges faster than the SBM. This is mainly because that the ASM adopts the true geometry of the boundary without approximation for computation unlike the SBM which uses in nature the straight line to approximate the segment geometry. It should be stressed that for such a 2D problem with very simple geometry, 200 boundary nodes generally should not be regarded as a small quantity. Therefore, the proposed ASM outperforms the SBM in terms of overall accuracy, efficiency, and robustness for the solution of the field potentials.

Again, Fig. 12 illustrates the relative error of the computed boundary normal fluxes versus the number of boundary nodes, demonstrating that the ASM also can solve the boundary physical quantities accurately and efficiently.

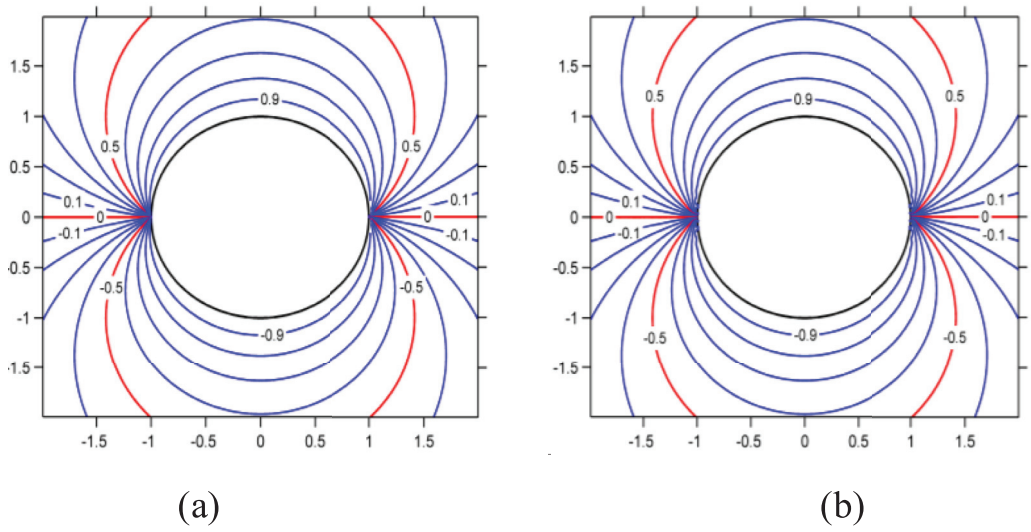

Fig. 8. The field potential solution: (a) exact results and (b) by using the proposed method.

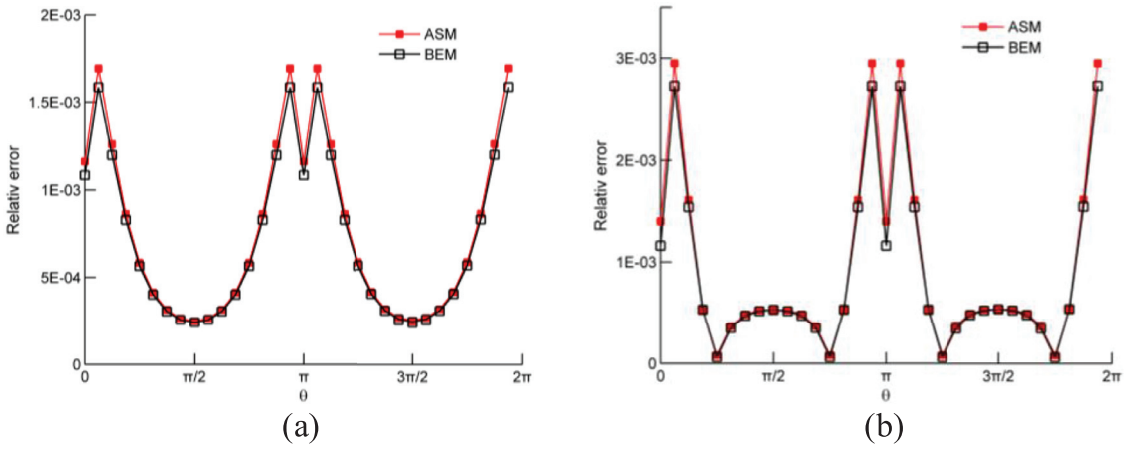

Fig. 9. The relative errors of the field solutions at radius $\rho = 2$: (a) potential and (b) flux $\partial u/\partial x_1$.

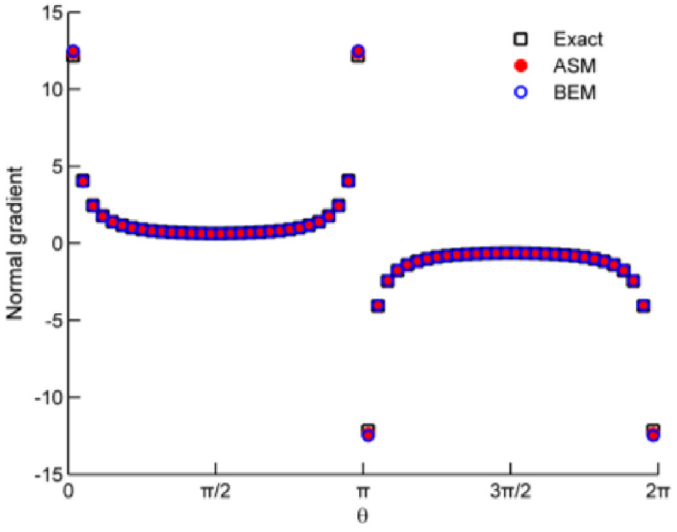

Fig. 10. The boundary normal flux solutions ($\partial u/\partial \boldsymbol{n}$) at 60 boundary nodes.

3.3. Multiply-connected domains with complex shapes

Example 5. This example investigates a mixed-type problem with multiply-connected domain, whose sketch is shown in Fig. 13. This problem has been used in Ref. [22] and its analytical solution is available as follows:

$$u = r^3 \cos(3\theta) \tag{34}$$

In this example, we suppose that the Neumann boundary conditions are prescribed on the boundary Γ_1 and Γ_3, and the Dirichlet boundary conditions on boundary both Γ_2 and Γ_4, as shown in Fig. 11. The numbers of boundary nodes on the four boundary parts Γ_1, Γ_2, Γ_3 and Γ_4 are taken as 7:1:1:1. Fig. 14(a) and (b) display the relative error surfaces of the field solutions for the potential and its derivative $\partial u/\partial x_1$ in the entire domain with 640 interior points, respectively. It can be clearly seen that good numerical accuracies can be obtained by the proposed method with only using 160 boundary nodes. Furthermore, Fig. 15(a) displays the relative error of the boundary potential solutions on Γ_1 and Γ_2 versus the number of boundary nodes, and Fig. 15(b) the relative error of the boundary normal flux solutions on Γ_1 and Γ_2 versus the number of boundary nodes. Hence it is observed from Fig. 15(a) and (b) that the ASM is stable, accurate and quickly convergent, and also has higher accuracy and convergence rates than the BEM with the increase of the boundary node number. This example il-

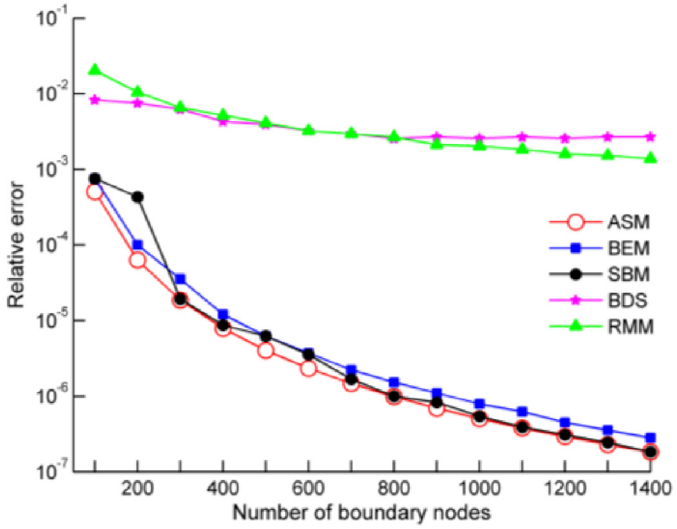

Fig. 11. Relatively error curves for the field potential solutions, respectively, by using the proposed ASM, BEM, SBM, BDS and RMM.

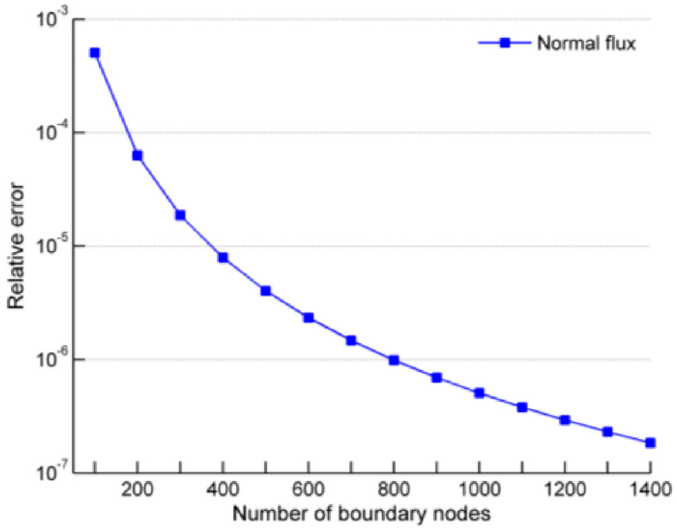

Fig. 12. Relative error of the computed boundary normal fluxes versus the number of boundary nodes.

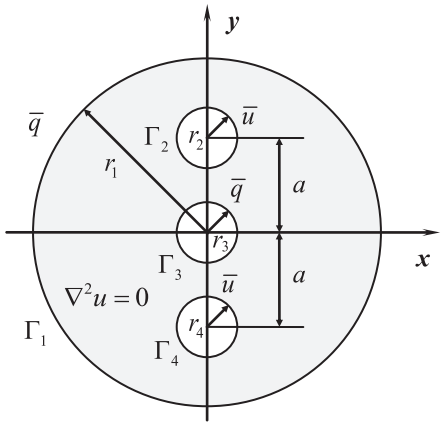

Fig. 13. Problem sketch ($r_1 = 2$, $r_2 = r_3 = r_4 = 0.25$ and $a = 1.0$).

lustrates that the proposed method works reasonably well for the multiply-connected domain problems.

Example 5. In the last example, an arbitrary-shape problem is considered, which is an example used in Ref. [22]. Problem sketch and the nodes distribution employing the proposed method are depicted in Fig. 16(a) and (b), respectively, in which the inner boundary Γ_2 is a circle with radius $r = 0.5$ and center at the origin and the outer boundary Γ_1 is a gear-shape curve, whose parametric equation is

$$\Gamma = \Big\{(r\cos\varphi, r\sin\varphi) : r = \frac{1}{n^2}\big[n^2 + 2n + 2 - 2(n+1)\cos(n\varphi - n\pi/2)\big], 0 \le \varphi \le 2\pi\Big\} \quad (35)$$

with $n = 6$. An analytical solution is available as follows [22]:

$$u(x, y) = e^x \cos y \quad (36)$$

The contour plot of the exact filed potential solutions is plotted in Fig. 17(a), and Fig. 17(b) depicts the filed potential results obtained by the proposed method with 120 boundary nodes. It can be found from Fig. 17(a) and (b) that the numerical results match the exact solutions well. Fig. 18(a) and (b) display the relative errors of the field solutions, respectively, for the potential u and the flux $\partial u/\partial x_1$ versus the number of boundary nodes by using the ASM and the BEM, in which the relative errors are yielded at 20 interior points uniformly distributed, according to φ, on the circle with radius $r = 0.9$ and center at the origin. We can observe from these two figures that the field solution accuracy and convergence

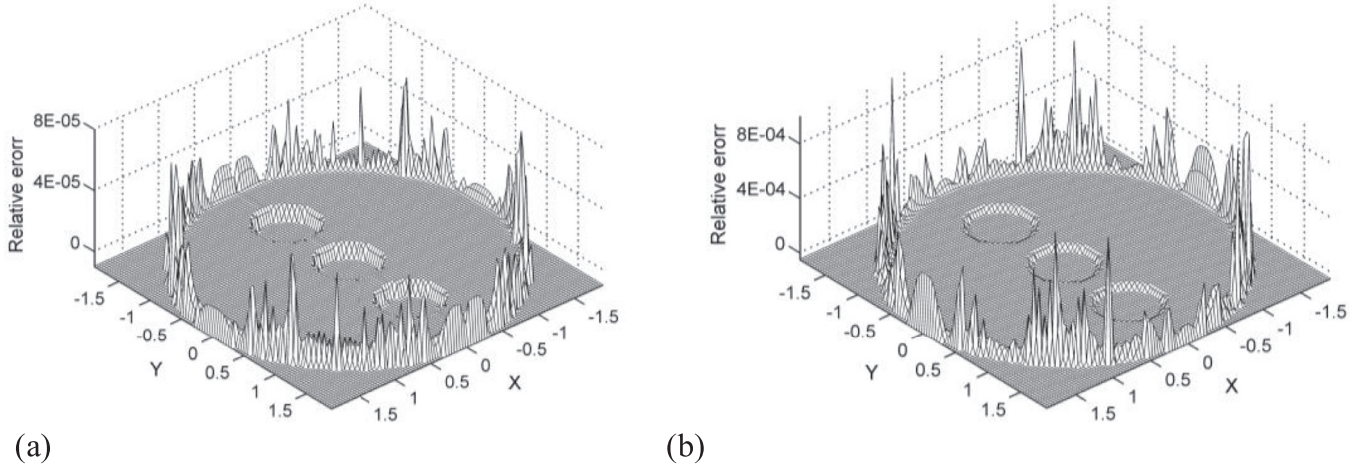

Fig. 14. Relative error surfaces for field solutions: (a) potential and (b) flux $\partial u/\partial x$ (160 nodes).

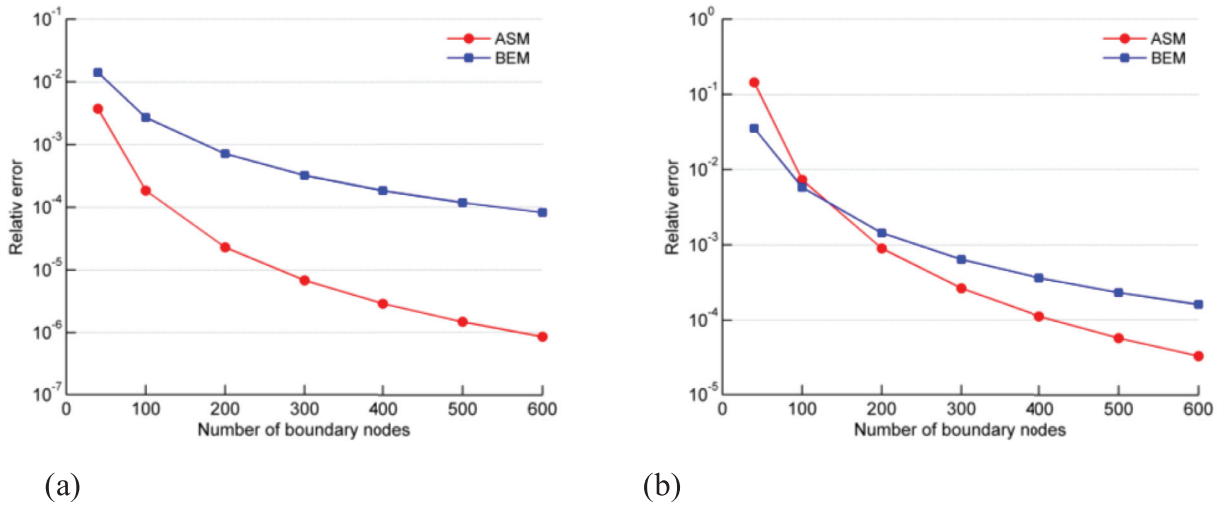

Fig. 15. Relative errors for the boundary quantities vs. the number of nodes: (a) potential on Γ_1 and Γ_3, (b) the normal flux $\partial u/\partial \boldsymbol{n}$ on Γ_2 and Γ_4.

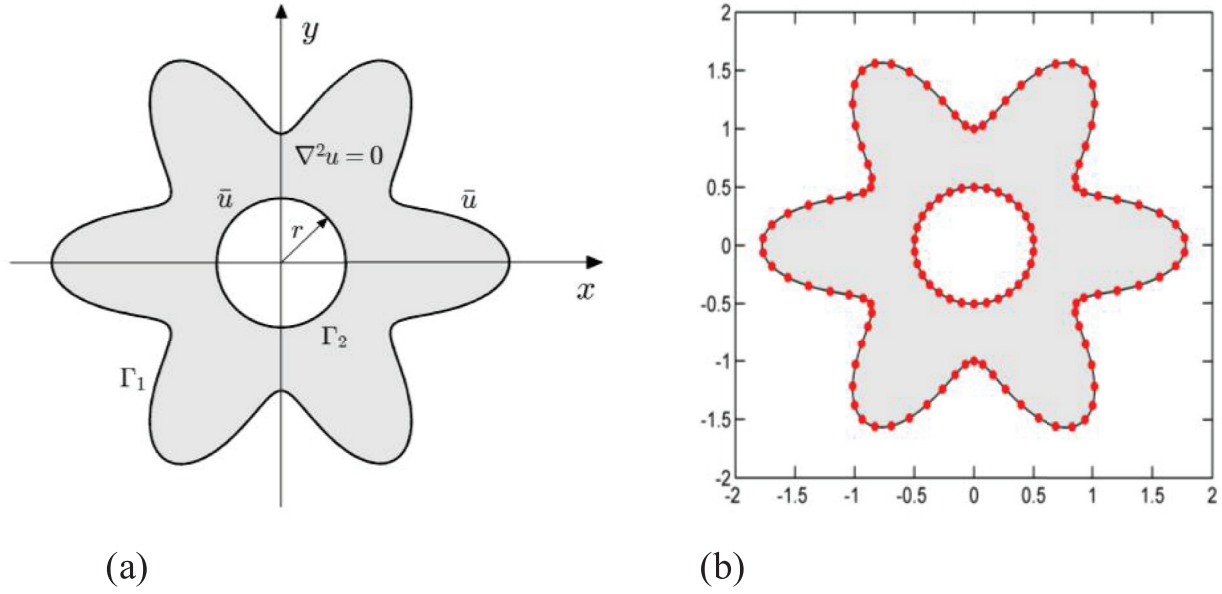

Fig. 16. (a) Problem sketch and (b) the nodes distribution (120 nodes).

rate of these two approaches are very close. Fig. 19 depicts the relative errors of the computed boundary flux $\partial u/\partial \boldsymbol{n}$ versus the number of boundary nodes by using the ASM and the BEM. It can be seen from this figure that the ASM has better accuracy and convergence rate than the BEM for the solution of the boundary flux, as the previous case in Fig. 15.

This test example demonstrates that the proposed ASM also works very well for the irregular domain problems.

4. Conclusions

In this paper, a new boundary-type meshfree method, termed average source method (ASM), is proposed to solve 2D Laplace problems. This method is based on coupling the RBIEs and the AST, which has the following key features:

1. The proposed ASM develops a new strategy to analytically compute diagonal coefficients of influence matrices, which are weakly singular or strongly singular, so that the problem can be solved only once, unlike the foregoing MFS-based type methods that apply a known solution to determine such diagonal coefficients, thereby doubling the solution procedure. This is an essentially crucial but very difficult issue for the boundary-type collocation schemes, and therefore great advance has been achieved by present work in this area.
2. Due to the using of the AST, the proposed ASM is a truly boundary-node method without involving any element or integration concept, unlike the aforementioned MLS-based methods that introduce the MLS-based meshless shape functions constructed elaborately into BIE to exploit the meshless attribute of MLS approximation, and but still need the calculation of boundary integrals. It is worth noting that this is a general methodology and also readily applicable to other or even singular BIEs. Some applications of the AST to other BIEs are already underway and will be reported in some subsequent papers.
3. For the present ASM, the true geometry of the boundary without approximation can be adopted for computation as long as the parametric representation of the domain boundary is given, as seen in the test examples in this paper.

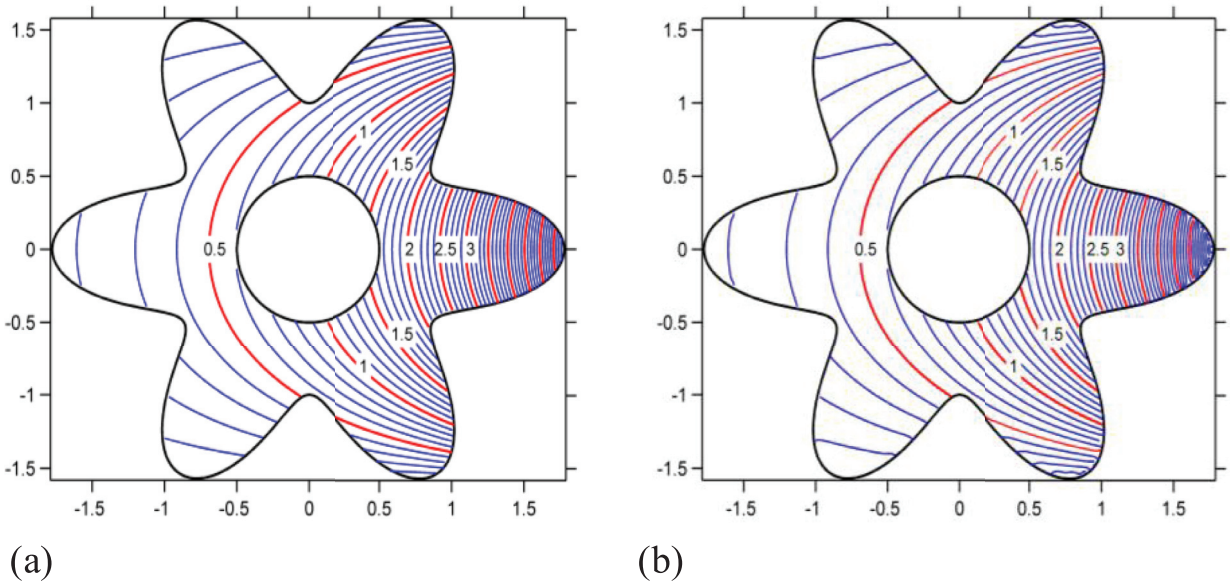

Fig. 17. The field potential solutions: (a) exact and (b) the proposed method (120 nodes).

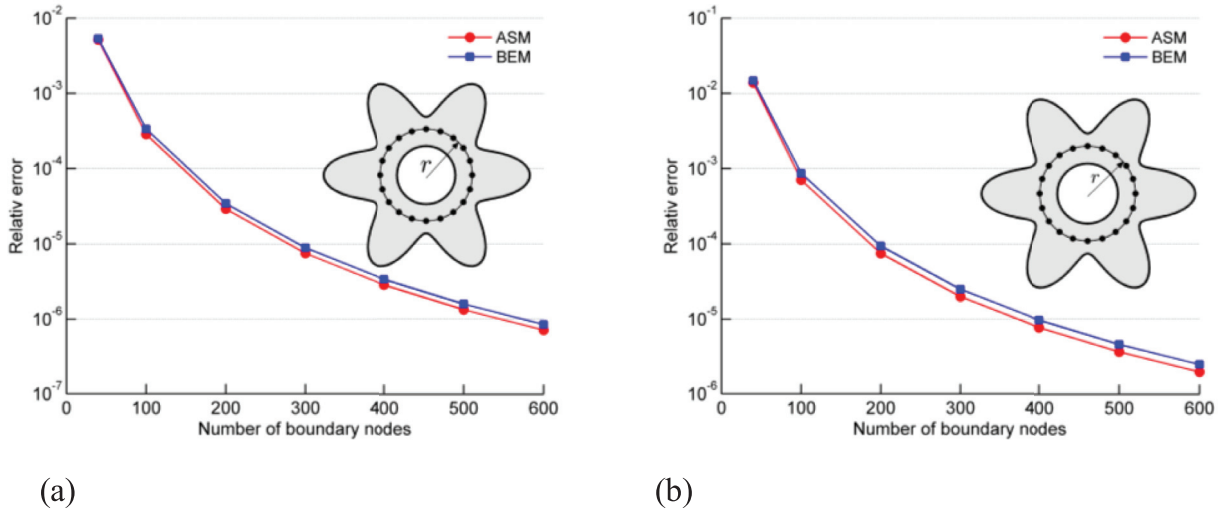

Fig. 18. Relative error for field solutions along the radius $r = 0.8$ vs. the number of nodes: (a) potential and (b) flux $\partial u/\partial x_1$. The symbols (•) in this Figure represent calculation points.

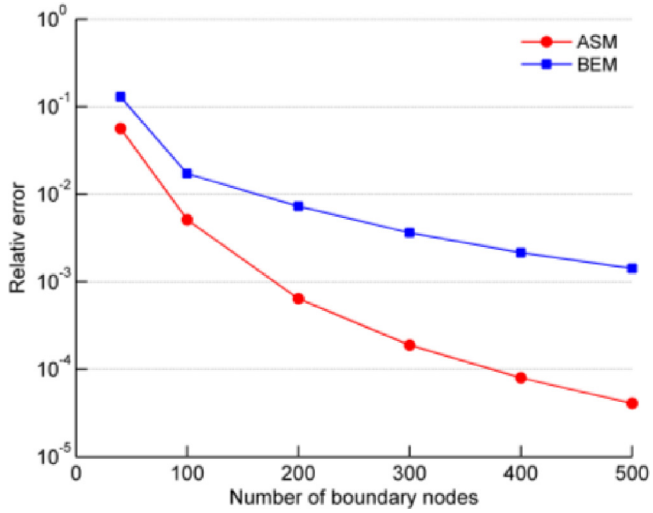

Fig. 19. Relative error for the boundary normal flux $\partial u/\partial \boldsymbol{n}$ vs. the number of boundary nodes.

Therefore, the ASM can seamlessly connect with parameter-based CAD technique, which is a demanding feature for the solution of practical engineering problems.

4. Unlike the MMFS, RMM and SBM, where the dimension (e.g., length or area) of a cell/segment need be evaluated and is generally obtained by a numerical integration as in Ref. [18,21–25], the present ASM does not involve such a problem. As stated before, the cells/segments in the ASM are only for computing the Jacobian values at the node.

Several category examples with different BCs and shapes of domain are presented to test the developed method. The numerical solutions obtained by present method agree very well with the exact solutions. From the figures of the various errors evaluation, such as the relative error, the absolute error and norm errors for the potential and its derivative solutions, we also can see that the numerical results exhibit a stable and rapidly convergent trend as the number of boundary nodes increases. All these features demonstrate that present method is efficient and accurate for the numerical analysis of 2D potential problems. Furthermore, the basic idea of the proposed method can be extended to the ASM

solution of other types of problems. Some works are already underway.

Moreover, it is observed that for the boundary value problem with discontinue BCs the solution accuracy and convergence rate of the ASM and the BEM are very close, while for the boundary value problem with continue BCs the ASM has better accuracy and convergence rates than the BEM with the increase of the boundary nodes number.

Acknowledgments

The support from the Natural Science Foundation of Shandong Province of China (ZR2010AZ003) is gratefully acknowledged.

References

[1] Katsikadelis JT. The boundary element method. Theory and applications. UK: Elsevier; 2002.
[2] Banerjee PK. The boundary element methods in engineering. Europe: McGRAW-HILL Book Company; 1994.
[3] Cheng AHD, Cheng DT. Heritage and early history of the boundary element method. Eng Anal Bound Elem 2005;29(3):268–302.
[4] Hwang WS. A regularized boundary integral method in potential theory. Comput Methods Appl Mech Engrg 2013;259:123–9.
[5] Gao XW, Davies TG. Boundary element programming in mechanics. Cambridge: Cambridge University Press; 2002.
[6] Liu YJ. Fast multipole boundary element method – theory and applications in engineering. London: Cambridge University Press; 2009.
[7] Sun HC, Zhang LZ, Xu Q, Zhang YM. Nonsingular boundary element method. Dalian University of Technology Press; 1999. (in Chinese).
[8] Liu GR. Meshfree methods: moving beyond the finite element method. 2nd ed. BocaRaton: CRC Press; 2009.
[9] Atluri SN. The meshless method (MLPG) for domain & BIE discretizations. California: Tech. Science Press; 2004.
[10] Mukherjee YX, Mukherjee S. Boundary methods: elements, contours, and nodes. Boca Raton: CRC Press; 2005.
[11] Li ZC, Lu TT, Hu HY, Cheng A. Trefftz and collocation methods. WIT Press; 2008.
[12] Fairweather G, Karageorghis A. The method of fundamental solutions for elliptic boundary value problems. Adv Comput Math 1998;9:69–95.
[13] Chen CS, Cho HA, Golberg MA. Some comments on the ill-conditioning of the method of fundamental solutions. Eng Anal Bound Elem 2006;30(5):405–10.
[14] Liu CS. An equilibrated method of fundamental solutions to choose the best source points for the Laplace equation. Eng Anal Bound Elem. 2012;36(8):1235–45.
[15] Chen W, Tanaka M. A meshless, integration-free, and boundary-only RBF technique. Comput Math Appl 2002;43:379–91.
[16] Fu ZJ, Chen W, Qin QH. Boundary knot method for heat conduction in nonlinear functionally graded material. Eng Anal Bound Elem. 2011;35:729–34.
[17] Chen JT, Chang MH, Hen KH, Chen IL. Boundary collocation method for acoustic eigenanalysis of three-dimensional cavities using radial basis function. Comput Mech 2002;29:392–408.
[18] Sarler B. Solution of potential flow problems by the modified method of fundamental solutions: formulations with the single layer and the double layer fundamental solutions. Eng Anal Bound Elem 2009;33:1374–82.
[19] Liu YJ. A new boundary meshfree method with distributed sources. Eng Anal Bound Elem 2010;34:914–19.
[20] Khambampati AK, Lee YG, Kim KY, Jerng DW. A meshless improved boundary distributed source method for two-phase flow monitoring using elecrical resistance tomography. Eng Anal Bound Elem 2015;52(3):1–15.
[21] Young DL, Chen KH, Lee CW. Novel meshless method for solving the potential problems with arbitrary domain. J Comput Phys 2005;209:290–321.
[22] Chen KH, Kao JH, Chen JT, Young DL. Regularized meshless method for multiply- connected-domain Laplace problems. Eng Anal Bound Elem 2006;30:882–96.
[23] Chen W, Wang FZ. A method of fundamental solutions without fictitious boundary. Eng Anal Bound Elem 2010;34:530–2.
[24] Chen W, Gu Y. An improved formulation of singular boundary method. Adv Appl Math Mech 2012;4(5):543–58.
[25] Gu Y, Chen W. Infinite domain potential problems by a new formulation of singular boundary method. Appl Math Model 2013;37:1638–51.
[26] Mukherjee YX, Mukherjee S. The boundary node method for potential problems. Int J Numer Meth Eng 1997;40:797–815.
[27] Zhang JM, Yao ZH, Li H. A hybrid boundary node method. Int J Numer Meth Eng 2002;53:751–63.
[28] Zhang JM, Qin XY, Han X, Li GY. A boundary face method for potential problems in three dimensions. Int J Numer Meth Eng 2009;80:320–37.
[29] Li XL. A meshless interpolating Galerkin boundary node method for Stokes flows. Eng Anal Bound Elem 2015;51:112–22.
[30] Lv JH, Miao Y, Zhu HP. Boundary node method based on parametric space for 2D elasticity. Eng Anal Bound Elem 2013;37:659–65.
[31] Liew KM, Cheng YM, Kitipornchai S. Boundary element-free method (BEFM) and its application to two-dimensional elasticity problems. Int J Numer Meth Eng 2006;65:1310–32.
[32] Zhang YM, Qu WZ. Average source meshless method. Joint international workshop on Trefftz method VI and method of fundamental solution II Taiwan; 2011.
[33] Zhang YM, Lv HX, Wang LM. Novel regularized boundary integral equations for potential plane problems. Appl Math Mech 2006;27(9):1165–70.
[34] Zhang YM, Liu ZY, Chen JT, Gu Y. A novel boundary element approach for solving the anisotropic potential problems. Eng Anal Bound Elem 2011;12:1181–9.
[35] Zhang YM, Liu ZY, Gao XW, Sladek V, Sladek J. A novel boundary element approach for solving the 2D elasticity problems. Appl Math Comp 2014;232(3):568–80.
[36] Liu CS. A BIEM using the Trefftz test functions for solving the inverse Cauchy and source recovery problems. Eng Anal Bound Elem 2016;62:177–85.